

論文 / 著書情報
Article / Book Information

Title	Optical and photoelectrical properties of oriented ZnO films
Authors	J. W. Tomm, B. Ullrich, X. G. Qiu, Y. Segawa, A. Ohtomo, M. Kawasaki, H. Koinuma
Citation	Journal of Applied Physics, Vol. 87, No. 4,
発行日/Pub. date	2000, 2
公式ホームページ /Journal home page	http://jap.aip.org/
権利情報/Copyright	Copyright (c) 2000 American Institute of Physics

Optical and photoelectrical properties of oriented ZnO films

J. W. Tomm^{a)}

*Max-Born-Institut für Nichtlineare Optik und Kurzzeitspektroskopie, Max-Born-Strasse 2A,
D-12489 Berlin, Germany*

B. Ullrich, X. G. Qiu, and Y. Segawa

*Photodynamics Research Center, The Institute of Physical and Chemical Research, 19-1399 Nagamachi,
Koeji, Aoba, Sendai 980-0868, Japan*

A. Ohtomo and M. Kawasaki

*Department of Innovative and Engineered Materials, Tokyo Institute of Technology, 4259 Nagatsuda,
Midori-ku Yokohama 226-8502, Japan*

H. Koinuma

*Materials and Structures Laboratory, Tokyo Institute of Technology, 4259 Nagatsuda, Midori-ku
Yokohama 226-8503, Japan*

(Received 2 June 1999; accepted for publication 10 November 1999)

ZnO films that have been used as active layers of optically pumped lasers are investigated by a number of optical and photoelectric techniques, such as transmission, reflectivity, photoluminescence and direct and alternating photocurrents. Homogeneity with respect to “bulk” and surface properties is evaluated. The spectral position of the lowest intrinsic exciton peak $E_x^{(A,B)}$ is determined to be at (3.323 ± 0.002) eV at 295 K. In spite of the rather small thickness of about $0.5 \mu\text{m}$, the samples do not exhibit strain-induced modifications of the optical properties at the band edge. A deep level is found to be responsible for the room temperature photocurrent, and excitonic features appear as absorption lines. On the other hand, excitonic photocurrent peaks are observed at low temperatures; however, the conduction mechanism still remains defect related. © 2000 American Institute of Physics. [S0021-8979(00)06804-3]

I. INTRODUCTION

ZnO is a classical wide-gap II–VI material with a band gap corresponding to an edge emission wavelength around 370 nm. It exhibits the Wurtzite structure and has a multiple valence band structure resulting in three band gaps, denoted A , B , and C gaps. Recently ZnO was proposed as a quantum-well material in $\text{ZnO}/\text{Zn}_{1-x}\text{Mg}_x\text{O}$ superlattices designed for use in future semiconductor lasers covering the ultraviolet (UV) spectral range below 370 nm.¹ Furthermore, reports on room temperature optically pumped lasing have been presented.^{2,3}

Increased film quality achieved by the introduction of laser molecular beam epitaxy (MBE),^{4,5} providing smooth layers which form an array of *coupled microcavities*,² plays a crucial role in this vast development. This technique allows *intentional alignment* of the c axis of the uniformly shaped hexagonal single crystallites.

The present study is motivated by the rapid growth in UV laser development and provides characterization of these laser samples. However, there are two additional important issues to be addressed.

First, there is a lack of knowledge on room-temperature band structure parameters of ZnO, such as the band gap E_g . This circumstance is directly addressed in Ref. 6 (cf. also references therein). There is much speculation in the litera-

ture about the influence of growth techniques and strain on the scatter of E_g values reported for ZnO. The high-quality oriented samples gives us the opportunity to perform spectroscopic experiments in order to clarify these questions. Our results yield the lowest free exciton energies ($E_x^{(A,B)}$) of (3.323 ± 0.002) eV at $T=295$ K. Assuming a free exciton binding energy of (60 ± 4) meV, the lowest $E_g^{(A,B)}$ position is found to be (3.383 ± 0.006) eV. The superscript (A,B) indicates that according to our experiments these gaps are not separable.

Second, if ZnO-based diode lasers are considered to be more than a motivation but as a serious goal, nonequilibrium carrier transport properties must be investigated. These results are presented here by photocurrent (PC) experiments, providing knowledge on lateral transport properties and electrical coupling of the crystallites in the 20–300 K temperature range.

II. EXPERIMENT

The five $1 \times 1 \text{ cm}^2$ shaped laser samples examined are formed by laser ablation using a KrF excimer (254 nm, 20 nm, 10 Hz).^{4,5} The laser beam was focused onto a ceramic ZnO target (five 9's). The material was ablated by a fluence of 0.6 J cm^{-2} and deposited on a sapphire (0001) substrate, which is kept at 550°C during the growth procedure. The typical back pressure of the molecular beam epitaxy (MBE) system used is 5×10^{-9} Torr. During the growth the pressure increases up to approximately 10^{-6} because of the oxygen

^{a)} Author to whom correspondence should be addressed; electronic mail: tomm@mbi-berlin.de

gas flux. All samples investigated have a *c*-axis orientation perpendicular to the substrate plane, as determined by x-ray diffraction. The film thickness varied between 200 and 800 nm. We concentrate the discussion on data achieved with one sample that has a thickness of $d=463$ nm. Pairs of electric contacts, separated by 1 mm, are implemented by In deposition at three positions on the samples. The external voltage applied for the PC measurements varied between 100 mV and 32 V. Apart from the absolute value of the PC signal no changes of the spectra are observed. Thus all measurements are done with a bias of 5 V, resulting in an electrical field of 50 V cm^{-1} . Methodical investigations carried out with both covered and intentionally illuminated contact pads make sure that our PC data are not influenced by the contacts. All PC measurements were made for constant photon flux using standard lock-in technique (ac measurements, modulation frequencies 10 Hz–3 kHz) and a picoammeter (dc measurements). PC, reflection (*R*), transmittance (*T*) and photoluminescence (PL) measurements were performed, using standard equipment, such as grating monochromators and charge coupled devices (CCD) multichannel analyzers. Since this article focuses mainly on room temperature experiments the spectral resolution was 1 meV. For the PL measurement we focused 50 μW of the 325 nm line of a HeCd laser to a spot size (FWHM) of about 500 μm , resulting in an intensity of 10 mW cm^{-2} . Finally it should be mentioned that the orientation of our film fixes the geometry of our spectroscopic experiments to $\mathbf{E} \perp c$, where \mathbf{E} is the vector of the electric field.

III. RESULTS

Sample homogeneity is tested at $T=295 \text{ K}$ by all the above-mentioned spectroscopic methods. We start by compiling the transmission data, which are measured at nine different positions uniformly distributed over the laser sample. A typical spectrum is shown in Fig. 1(a), cf. right ordinate scale. The peak is positioned at $(3.323 \pm 0.002) \text{ eV}$. The extremely small standard error of estimation for multiple measurements across the sample indicates excellent homogeneity. Figure 1(a) shows an additional spectrum. It is calculated as the *ratio* of two PC spectra measured at modulation frequencies of 10 Hz and 3 kHz. Such a PC ratio spectrum basically reveals the same information as the phase of the lock-in PC measurements, i.e., providing an insight into (slow) kinetics. The original spectra, from which the ratio was calculated, are shown in Fig. 1(b). A detailed discussion of these PC ratios will be given in Sec. IV, however, it is clear that these peaks are at spectral positions where the fastest PC contribution dominates. Obviously both spectra, *T* and PC ratio, exhibit peaks at the same spectral position, indicating that the strongest absorption and the fastest PC contribution have the same origin. We wish to stress that this statement is valid for all three positions where pairs of In electrodes have been deposited on the sample. Furthermore, we find the full correspondence between *T* and PC ratio peaks are maintained for the low-temperature measurements as discussed in Sec. III. It should be noted that the PC ratio peak is very close to the spectral position where the original

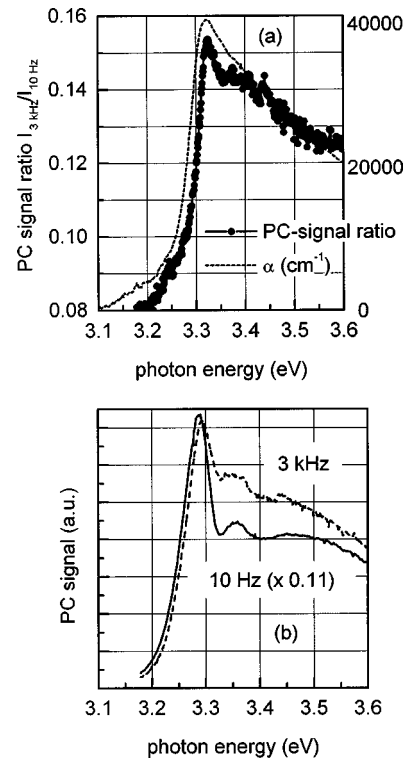


FIG. 1. (a) Absorption coefficient (right ordinate scale) and photocurrent signal ratio vs photon energy for a 463 nm thick oriented ZnO laser film. The photocurrent signal ratio was calculated by dividing the curves given in (b). (b) Photocurrent spectra from the same sample obtained by lock-in technique for two different modulation frequencies.

PC spectra [cf. Fig. 1(b)] have a pronounced minimum. In addition a certain PC peak shift towards higher energies for increasing modulation frequencies is found. Thus, a very early conclusion can be drawn: Processes exhibiting slow kinetics govern room temperature photoconductivity in ZnO laser samples. Here the term slow refers to the inverse modulation frequency (0.3–100 ms).

Having established the extremely uniform distribution of the spectral position of the absorption edge across the samples, we now address optical properties that are rather nonuniformly spread. Figure 2(a) and 2(b) show normalized, room temperature PL and *R* spectra from two different sample positions exactly defined by the position of two pairs of PC electrodes. The spectral position of the absorption peaks, PC ratio peaks, and the PC peak are marked by symbols. Obviously the PC peaks follow the shift of the PL and *R* spectra. As mentioned, the spectral positions of the PC ratios and the transmission peaks are the same in Figs. 2(a) and 2(b). However, PL, PC, and *R* features are *simultaneously shifted with respect to these fixed spectral positions*. Comparing Figs. 2(a) and 2(b) the relative shifts are 15–20 meV. The absolute Stokes shift with respect to the absorption peak at $(3.323 \pm 0.002) \text{ eV} (E_x^{(A,B)})$ is 12–40 meV. In addition the spectral width of the PL and *R* features also changes. Obviously, the spectra in Fig. 2(b) are broadened and shifted towards lower energies. For both positions the PC peak exhibits the same arbitrary shift as the PL and *R* features. In Fig. 2(a) line positions for $E_x^{(A,B)}$, $E_x^{(C)}$, $E_g^{(A,B)}$ and $E_g^{(C)}$ taken from the article of Sobolev *et al.* are shown.⁷

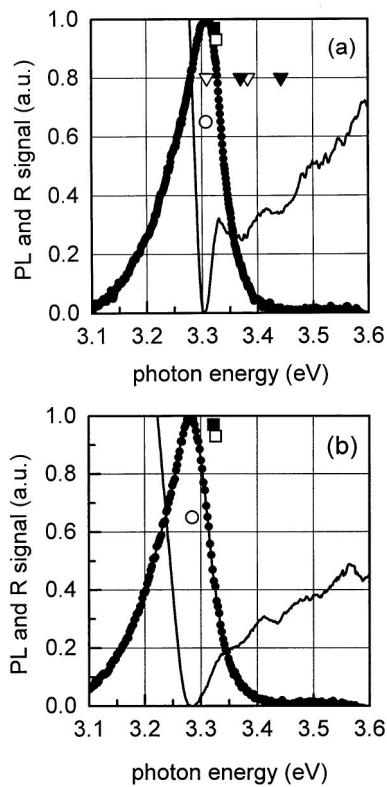


FIG. 2. (a) Reflectivity (solid line) and photoluminescence (full circles) vs photon energy for one fixed position on the sample. The squares give the position of E_x determined by absorption (full square) and PC signal ratio (open square), whereas the triangles are the positions of the excitons (open triangles) and band edges (full triangles) according to Ref. 7. The open circle indicates the spectral position of the ac PC spectrum measured with a modulation frequency of 28 Hz. (b) Reflectivity (solid line) and photoluminescence (full circles) vs photon energy for another fixed position on the sample separated about 5 mm from the position in (a). The squares give the position of E_x determined by absorption (full square) and PC signal ratio (open square). The open circle indicates the spectral position of the ac PC spectrum measured with a modulation frequency of 28 Hz.

To our knowledge, these are the most reliable room-temperature data reported so far for “perfect”⁷ *bulk* materials. Note the remarkable agreement with the absorption patterns visible in the *R* spectra, commonly called “exciton gap”

Figure 3(a) shows ac PC spectra for the temperature range 20–295 K in a semilogarithmic display. Additionally, absorption and PC ratio peaks are marked by symbols. In remarkable agreement with Ref. 7, we find the temperature coefficient (100–295 K) to be $(2.9 \pm 0.1) \times 10^{-4} \text{ eV K}^{-1}$. Obviously, the well-pronounced room temperature PC peak [cf. Figs. 1(b) and 3 (top)] appears significantly below the room temperature band edge. In addition to finding a remarkable modulation frequency dependence of the room temperature PC peak, we provide a second and independent argument for a defect-related nature of this peak. The depth of the corresponding defect is 100–150 meV and its nature will be the subject of future work. Figure 3(b) shows the 20 K spectrum [at the bottom in Fig. 3(a)] in a linear plot. The three relevant exciton positions $E_x^{(A)}$, $E_x^{(B)}$ and $E_x^{(C)}$ are extracted from the classic papers by Thomas,⁸ Liang and Joffe,⁹ and Hümmer.¹⁰ The absence of a significant $E_x^{(C)}$ contribution is

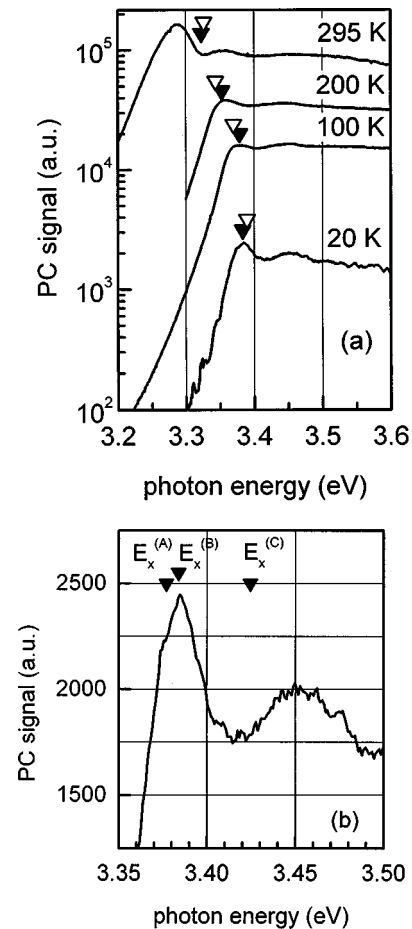


FIG. 3. (a) ac PC spectra for different temperatures (modulation frequency 28 Hz). The triangles give the position of E_x determined by absorption (full triangle) and PC signal ratio (open triangle). (b) ac photocurrent spectrum at $T=20 \text{ K}$ (modulation frequency 28 Hz). The symbols represent the positions of E_x for the A, B, and C gaps taken from Ref. 8–10.

caused by our experimental geometry ($E \perp c$). This is clear evidence of the high orientation degree of the laser sample.

We compare our low temperature thin-film data with “classical exciton data” in order to show that our samples are high-quality layers with “bulk-like” optical properties, in which strain or other specific parameters do not influence the gap position. This knowledge is very important for proceeding from sample-specific conclusions to more general ones. The spectra reveal that excitonic effects significantly influence both high- and low-temperature PC. They appear as lines in the low-temperature spectra, whereas the room-temperature spectra are influenced by reabsorption patterns. The transmission data confirm the positions of the exciton lines.

The previous findings indicate the involvement of very slow defect-related processes in the formation of the PC signals. As a consequence, we decided to measure dc PC spectra. Figure 4 exhibits the data after dark current subtraction. Again the spectral positions of the transmission and PC ratio are marked. The spacing (determined by line shape fits) between the peaks [Fig. 3(b)] and the minimum (Fig. 4) is slightly increased from about 65–68 meV at 20–295 K, respectively. Since this spacing is determined by several pa-

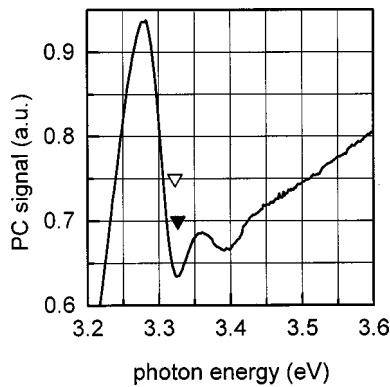


FIG. 4. dc photocurrent spectrum at $T=295$ K. The triangles represent the positions of E_x determined by absorption (open) and PC signal ratio (full).

rameters, such as the temperature dependence of the exciton binding energy (between 59 and 61 meV for the different gaps, cf. Ref. 11) and the thermal broadening, we tentatively consider this shift as a source of error for the E_g determination. However, a certain potential for obtaining information about *intrinsic* features is visible. In addition dc PC spectra are measured for low temperatures. We should note that the increase of the sample resistance toward lower temperatures was about the same for ac and dc measurements.

IV. DISCUSSION

Experimental arguments for excitonic contributions to the high- and low-temperature PC spectra have been presented. We have demonstrated that excitonic contributions are the “fastest” PC contributions [cf. Fig. 1(a)] in the thin films investigated. These observations need to be understood at least qualitatively. A general quantitative description can be found in textbooks.^{12,13} Lack of detailed knowledge about many parameters, such as defects (depth, concentration), mobilities and others, however, leads to difficulties in obtaining additional physical insight by using the models discussed there.

Creation of a PC signal demands the spatial separation of carrier pairs generated by absorption. Since our ZnO samples are free of macroscopic gradients (we find no electromotive force without applying a bias), an external electric field separates electrons and holes. Therefore, excitons as quasineutral particles do not directly contribute to the PC signal. However, there are several indirect ways. Among them scattering at shallow and deep defects or Urbach-tail states (and their ionization) is probable. Defect states, situated below E_x , may provide PC contributions via various “hopping,” PC mechanisms. This is experimentally proven for the samples by the pronounced below-gap PC peak at 295 K. It is known that the PC signal is roughly proportional to the mobility μ of the nonequilibrium carriers and to their concentration δn . Since our samples show a certain transmission even at E_x , the condition $\alpha \times d \ll 1$ holds surely for defect levels [cf. Fig. 1(a)]. The term “mobility” here must be understood as ‘effective macroscopic’ mobility μ_{eff} (drift velocity divided by electric field strength) and differs for

different defect related conduction channels. Consequently, we assume that the PC signal is proportional to $\alpha \times \mu_{\text{eff}}$.

Taking into account the spectral dependence of α [Fig. 1(a)], all observations will be consistently explained.

(i) *Room temperature PC is directly created* by optical transitions via deep levels [cf. Fig. 1(b)]. Although α for deep levels is small, extremely high μ_{eff} values (caused by the long lifetime) produce the deep-level PC peak. At E_x , the excitonic absorption significantly reduces the number of carriers being absorbed by deep levels. However, a part of the carriers absorbed at E_x become scattered again into states providing conductivity. On the other hand, the net losses dominate and create the excitonic absorption pattern within the PC spectrum.

(ii) *For low temperatures* the main defect related PC line freezes out. Other defect-related PC channels do exist further and form, e.g., the long tails in Fig. 3(a) by direct absorption. Strong absorption at E_x provides many carrier pairs and the fraction which becomes scattered into more efficiently conducting defect states (situated at higher energies than the deeper levels) produces the exciton peak. Between E_x and E_g , α is expected to become smaller, resulting in a dip. The broad interband feature centered at 3.45 eV [Fig. 3(b), $T=20$ K] is explained by the increase of μ_{eff} at the tail states (and reduction of μ_{eff} above E_g caused by the small interband lifetime) and /or surface recombination.

(iii) Finally we address the “slow” PC kinetics, i.e., the *PC ratio spectrum*. The general reduction of the PC signal with increasing modulation frequency [cf., Fig. 1(b)] is caused by the RC low pass filter formed by the capacitance and resistance of sample and lock-in amplifier.

The additional photon energy dependence [Fig. 1(a)] of the PC time constant is explained as follows. Generally, there is a tendency that carriers in deeper levels have longer lifetimes than those at shallower levels. Furthermore, α of shallower levels or tail states, i.e., states closer to E_x , is larger [cf. Fig. 1(a)]. Hence, towards E_x the number of carriers being in faster contributing states (e.g., shallower levels) increases. At E_x the excitons become scattered into the fastest contributing states (e.g., shallower levels or tail states), resulting in a peak in the PC ratio spectrum. The strong absorption additionally reduces the number of carriers directly excited by transitions via levels that display slower kinetics. Above E_x , α decreases. Therefore the excited density of slower contributing defect states increases, slowing down the kinetics of the PC process. Furthermore trapping and surface recombination play an increasing role.

Finally, it should be mentioned again that we have discussed here slow PC kinetics that reflect primary kinetics (such as excitonic ones). Our results do not allow any conclusions about the kinetics of the *primary* processes, except that they are “fast” compared to the modulation frequency used in our ac measurements.

In Sec. III we have shown excellent lateral sample homogeneity with respect to the excitonic absorption peak at (3.323 ± 0.002) eV. Together with the sound agreement of our low-temperature data (Sec. III) with literature data^{8–10} obtained from bulk crystals, we conclude that the band structure of our laser films is not affected by strain. We show

experiments (cf. Sec. III) revealing Stokes shifted PL and *R* patterns (Fig. 2). With respect to (3.323 ± 0.002) eV the shift is 12–40 meV. Despite this shift the PL data in Fig. 2, particularly Fig. 2(a), indicate excellent sample properties. The deep level PC peak shifts simultaneously with the PL- and *R* spectra. Thus, a certain coupling between the defect behavior (depth and/or concentration) and the PL and *R* pattern is very likely. One could speculate, whether band-gap renormalization in surface layers, localization effects or surface excitons (at room temperature?) cause the effect. Further work will clarify these open questions.

A very practical conclusion can be drawn from our work as well. Reflection patterns from ZnO are not always as reliable as necessary for the investigation of intrinsic material properties. Consequently, we propose to shift the $E_x^{(A,B)}$, $E_x^{(C)}$, $E_g^{(A,B)}$ and $E_g^{(c)}$ values given by Sobolev *et al.* [cf. Fig. 2(a)]⁷ by at least 10 meV toward higher energies.

V. SUMMARY

We report optical and photoelectrical properties of oriented ZnO films on sapphire that have served as active layers for optically pumped UV lasers.² Our data show *excellent lateral sample homogeneity* of the laser films. Despite the fact that the samples investigated are thin films, strain does not notably affect the band structure of the ZnO film in comparison to bulk material. However, surface properties are less homogeneously distributed spatially.

The spectral positions of $E_x^{(A,B)}$ as well as $E_g^{(A,B)}$ are determined to be (3.323 ± 0.002) and (3.383 ± 0.006) eV, respectively. We propose shifting the values given by Sobolev *et al.*⁷ by at least 10 meV toward higher energies.

Photocurrent spectra of oriented ZnO films are measured in the 20–295 K temperature range. All spectra are governed by various defect-related conduction mechanisms. Excitonic

features appear either as absorption lines (295 K) or as direct PC lines (low temperatures). In the latter case, however, the transport mechanism itself is defect related.

The finding that the different PC contributions have different time constants can be used as a characterization tool for thin film samples. We have established that the fastest PC contribution always appeared at E_x .

ACKNOWLEDGMENTS

This work was partly supported by JSPS Research for the Future Program in the area of Atomic-Scale Surface and Interface Dynamics (Grant No. RFTF96P00205). One of the authors (J. W. T.) wishes to express his gratitude to the Photophysics Group and Y. Segawa at The Institute of Physical and Chemical Research (RIKEN) for funding his work in Japan.

¹A. Ohtomo, M. Kawasaki, Y. Sakurai, I. Ohkubo, R. Shiroki, Y. Yoshida, T. Yasuda, Y. Segawa, and H. Koinuma, *Mater. Sci. Eng.*, B **56**, 263 (1998).

²Z. K. Tang, G. K. L. Wong, P. Yu, M. Kawasaki, A. Ohtomo, H. Koinuma, and Y. Segawa, *Appl. Phys. Lett.* **72**, 3270 (1998).

³D. M. Bagnall, Y. F. Chen, Z. Zhu, T. Yao, M. Y. Shen, and T. Goto, *Appl. Phys. Lett.* **73**, 1038 (1998).

⁴H. Koinuma and M. Yoshimoto, *Astron. Astrophys., Suppl. Ser.* **75**, 308 (1994).

⁵H. Koinuma, M. Kawasaki, and M. Yoshimoto, *Mater. Res. Soc. Symp. Proc.* **397**, 145 (1996).

⁶V. Srikant and D. R. Clarke, *J. Appl. Phys.* **83**, 5447 (1998).

⁷V. V. Sobolev, V. I. Donetskiikh, and E. F. Zagainov, *Sov. Phys. Solid State* **12**, 646 (1978).

⁸D. G. Thomas, *J. Phys. Chem. Solids* **15**, 86 (1960).

⁹W. Y. Liang and A. D. Joffe, *Phys. Rev. Lett.* **20**, 59 (1968).

¹⁰K. Hümmer, *Phys. Status Solidi* **56**, 249 (1973).

¹¹Landolt-Börnstein, *New Series III*, Vol. 22a, p. 161 (Springer, Berlin, 1987).

¹²K. Seeger, *Semiconductor Physics* (Springer, Berlin, 1997).

¹³K. H. Herrmann, *Der Photoeffekt* (Vieweg Lehrbuch, Braunschweig, 1994).